ACOUSTIC EMISSION DURING FLUID INJECTION INTO ROCK

James D. Byerlee and David Lockner
U.S. Geological Survey
Menlo Park, California, 94025

Summary

The source locations of acoustic emission events were determined during the injection of water into a sample of Weber sandstone subjected to constant confining pressure and differential stress. For the first 10,000 minutes, the shocks were randomly distributed throughout the sample. During the next 460 minutes, they originated at the end of the sample where the water was being injected. Failure then occurred rapidly, and the fracture front advanced through the sample as water flowed through the fractured material of increased permeability, maintaining a low effective stress at the fracture front. It is notable that the most intense activity occurred at the fracture front, and once the fracture front passed a region, the acoustic emission decreased even though the differential stress was maintained at a constant value and the pore pressure in that region increased as water flowed into the sample.

Introduction

Acoustic emission has been used in the field of material science as a nondestructive test for structural flaws and fatigue. If the source of the events can be located, the sites of potential weakness in the structure can be identified. This technique has been applied to the assessment of the structural integrity of pressure vessels for nuclear and petroleum industries, rocket motor casings, bridges, buildings, and wooden beams (Liptai *et al.*, 1972).

In rock mechanic studies Mogi (1972) located the source of acoustic-emission events during failure of rock subjected to a bending moment and thus was able to study the growth of tension fractures preceding catastrophic failure. Scholz (1970) studied the acoustic emission in granite under uniaxial compression and by using six transducers attached to the surface of the sample was able to locate some of the acoustic-emission events prior to shear failure.

We have developed a system to study acoustic emission in rock which is subjected to high confining pressure, differential stress, and pore pressure. The purpose of this paper is to describe the experimental apparatus and the method that we use to locate, in three dimensions, the origin of the acoustic-emission events. We will also report the results of an experiment designed to study the acoustic emission which occurred during the injection of fluid into a sandstone

sample that was under confining pressure and differential stress.

Mechanical System

A schematic diagram of the system is shown in Figure 1. The sample represented by the stippled region in the center of the figure is a cylinder of rock 19 cm long by 7.6 cm in diameter. The reason for using such large samples was to increase the relative accuracy of the location of the acoustic-emission events. The relative error in location is determined by the absolute errors divided by the diameter of the sample. Thus the more accurate the timing and the larger the sample size, the smaller the relative error.

In order to prevent the confining pressure fluid from entering the pores of the rock, the sample was jacketed in a polyurethane sleeve 0.475 cm thick. Lead zirconate piezoelectric transducers were attached to the ends of hardened steel plugs 0.792 cm in diameter. The other ends of the plugs were ground to the same radius of curvature as the rock cylinder. The plugs were attached to the sample and sealed to the holes through the jacket with epoxy cement. The jacket was sealed to hardened steel end plugs with steel clamps. Both end plugs are hollow so that the pore fluid could be pumped through the sample. The leads from the 6 transducers were connected to insulated conical pins which fitted into holes bored in the larger end plug.

The confining pressure fluid was kerosene and was pumped into the pressure vessel through the lower hole in the side of the vessel by a pump that has an upper limit of 5 kb. The upper hole in the side of the vessel was used to bleed off air as the pressure vessel was filled with liquid.

The differential stress on the sample was applied by advancing the piston with a hydraulic ram having a capacity of 750,000 kg force. The confining pressure and pore-fluid injection pressure were visually monitored outside the pressure vessel with heise gages. The axial load on the sample was measured with a load cell and the axial displacement of the piston was measured with a DC DT transducer.

The outputs of the load cell and differential transducer were fed into an x-y recorder so that the stress strain curve during loading and deformation of the sample was recorded directly. The output of pressure transducers attached to the confining pressure and pore fluid pressure lines were fed into strip chart recorders so that a permanent record of these pressures was obtained.

The system is servo-controlled so that the confining pressure, pore-fluid injection pressure, and differential stress can be maintained at any desired value during an experiment.

Electronic System

The outputs of the piezoelectric transducers which had resonant frequencies of 600 khz were fed into wide-band preamplifiers and the amplified signals were then fed into a data acquisition and recording

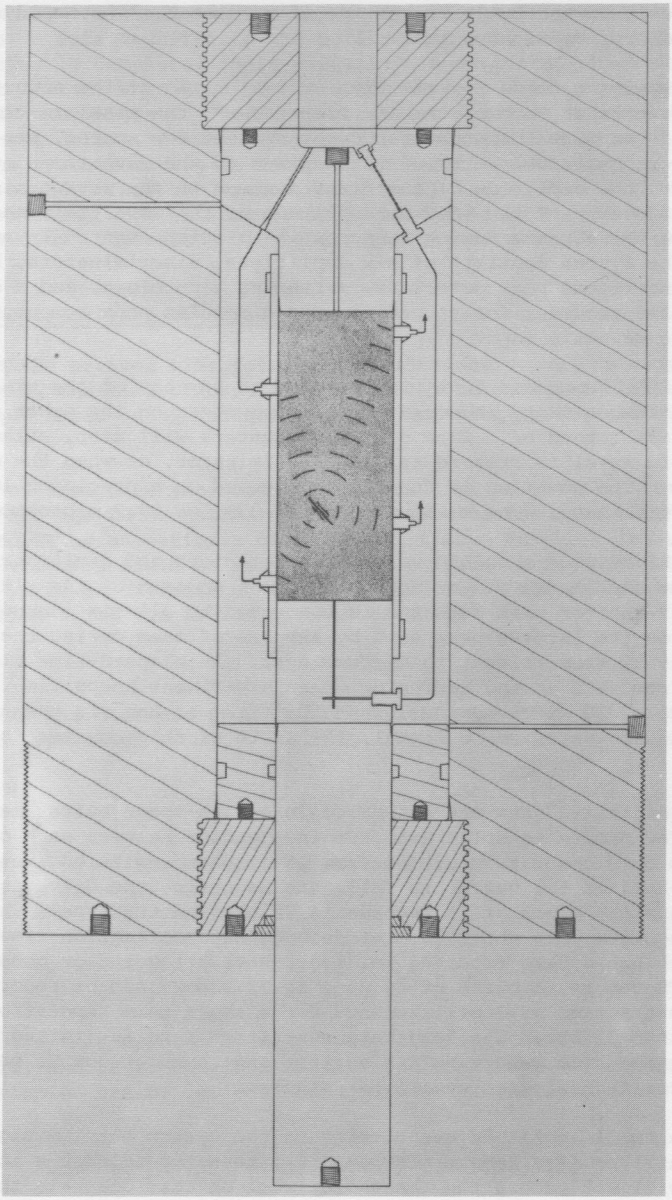

Fig. 1. Schematic diagram of the loading system. The sample shown shaded is contained within a pressure vessel. Load is applied to the sample with a piston which moves through an O-ring seal.

system, designed and built to our specifications by "The Nanodyne Corp., Sudbury, Massachusetts".

The system records the relative arrival times of the acoustic-emission events at each of the six transducers, the absolute time of arrival of the signal at the transducer nearest the source, the sign (positive or negative) of the first maximum in the wave train at each transducer, the amplitude of the first maximum in the wave train at each transducer, and the maximum amplitude of the wave train seen by any of the transducers during an acoustic-emission event. In more detail, the system consists of six amplifiers, discriminators, high speed counters and peak detectors, a running time clock, and a data formater and recorder for recording edited results on a computer-compatible magnetic tape.

When the threshold level is exceeded on any one of the six input channels, its polarity is noted and time counters on the other five channels are turned on. Each of these counters will stop, either when a threshold level is crossed at its discriminator, or when the counter overflows. The counting is done decimally and on a precision 10 MHZ (100 ns) time base. The maximum count is 999, or 99.9 microseconds.

Six high-speed absolute-value peak detectors and digitizers detect the amplitudes of the very first peak on each of the six channels. Another peak detector is connected to all six channels and records the largest peak seen by any one of them during the entire time interval from trigger to system reset. An elapsed-time clock started from zero at the beginning of an experiment keeps time in increments of 10 microseconds. When the first of the six channels reports an above-threshold signal, the state of this counter is recorded.

The digitized data are assembled in a high-speed buffer memory. This buffer memory is split into two independent halves, each of which can hold the data recorded from 16 acoustic-emission events. When one-half of the buffer is full, the magnetic tape drive is started and the block of 16 records is written on the tape. The system requires only about 30 microseconds data collection time after all six channels have reported in, i.e., have triggered or gone over-range. Therefore, a burst of as many as 32 shocks can be recorded in as short a time as 2 milliseconds for a short term repetition rate of more than 25 khz. The long-term repetition rate is limited by the transfer time from memory buffer to tape and is about 300 Hz or about 18,000 acoustic-emission events per minute.

If a small-amplitude event triggers the system but the signal, when it arrives at a remote station, is attenuated to such a low level that it will not exceed the threshold level on that channel, the counter will go overrange. The system contains logic circuitry to detect this condition and the data collected during the event is ignored. If external electronic interference triggers the system, more than one channel will trigger simultaneously. The logic circuitry detects such events and automatically rejects this data as well.

When all six channels have reported in (been triggered or gone overrange) a data transfer to the buffer memory is begun. As soon as the transfer is complete, logic circuitry is activated which detects the first instant when none of the channels sees a larger-than-threshold input signal. When this condition persists for the duration of a pre-set delay (10-100 microsecond), a signal is generated which clears the system, making it ready to accept the next acoustic-emission event. Thus the system waits until there is no activity before switching back on so that it is triggered on a real event undistorted by reflections or the decaying wave train of the previous events.

Mathematical Analysis of Arrival Time

From the arrival time data at the transducers, we can compute the location and time of each event, and the seismic velocity by using a technique employed by seismologists in locating earthquake hypocenters.

Let us designate the measured arrival time at the i^{th} station by t_i. Let XE, YE, ZE be estimates of the space coordinates of the hypocenter and TE be an estimate of the event time. Further, let us assume that the velocity field is isotropic and uniform throughout the sample. Then let VE be an estimate of the wave velocity. The calculated arrival time $\hat{t}_i$ at the i^{th} station is given by

$$\hat{t}_i = TE + D_i/VE \tag{1}$$

where D_i is the distance from the i^{th} station (X_i, Y_i, Z_i) to the estimated hypocenter

$$D_i = \left[(XE - X_i)^2 + (YE + Y_i)^2 + (ZE - Z_i)^2\right]^{1/2} . \tag{2}$$

A best estimate of the hypocenter can be made by minimizing the time residual, R, given by

$$R = \left[\sum_{i=1}^{6} (t_i - \hat{t}_i)^2\right]^{1/2} \tag{3}$$

We can solve this problem by repeatedly altering the variables XE, YE, ZE, TE, and VE to obtain a smaller and smaller R. The change in these variables can be called the adjustment vector as defined by the equation

$$dS = \left[d[TE], d[XE], d[YE], d(ZE), d(VE)\right] . \tag{4}$$

We can improve our first estimate by adding to it the adjustment vector.

$$\begin{aligned} \text{Improved TE} &= \text{TE} + \text{d[TE]} \\ \text{Improved XE} &= \text{XE} + \text{d[XE]} \\ \text{Improved YE} &= \text{YE} + \text{d[YE]} \\ \text{Improved ZE} &= \text{ZE} + \text{d[ZE]} \\ \text{Improved VE} &= \text{VE} + \text{d[VE]} \end{aligned} \tag{5}$$

Then by using this new estimate we can calculate a new adjustment vector and further improve our estimate, repeating the process until we have found a minimum for R. Further, the magnitude of R gives an estimate of the uncertainty of the solution to the event location.

If the velocity field in the rock were truly isotropic and if the arrival times were known exactly (arrival times are rounded off to the nearest tenth of a microsecond), 5 arrival-time measurements would be sufficient to locate the acoustic-emission event exactly because we have 5 measurements with 5 unknowns. In this case, R would be zero. Since various measurement errors are present, some redundancy is required to obtain a measure of the reliability of the solution. Therefore we need at least 6 arrival times to solve for the variables. Then the magnitude R given by equation (3) gives us an estimate of the uncertainty of the solution of the even location.

The method that we use is to form the Taylor expansion of $\hat{t}_i$ in terms of TE, XE, YE, ZE, and VE. Ignoring all differentials higher than the first order, we obtain

$$\hat{t}_i = \text{TE} + \frac{\partial \hat{t}_i}{\partial (\text{TE})}\, d(\text{TE}) + \frac{\partial \hat{t}_i}{\partial [\text{XE}]}\, d[\text{XE}] + \frac{\partial \hat{t}_i}{\partial [\text{YE}]}\, d[\text{YE}] + \frac{\partial \hat{t}_i}{\partial (\text{ZE})}\, d[\text{ZE}] + \frac{\partial \hat{t}_i}{\partial (\text{VE})}\, d[\text{VE}] \,. \tag{6}$$

If we substitute $\hat{t}_i$ given by equation (6) into the equation

$$R^2 = \sum_{i=1}^{6} (t_i - \hat{t}_i)^2 \,, \tag{7}$$

differentiate R^2 with respect to the five variables in the adjustment vector, and equate the results to zero, we obtain five simultaneous equations (called the normalized equations) given by

$$\begin{bmatrix} N & CX & CY & CZ & CV \\ CX & CX^2 & (CX)(CY) & (CX)(CZ) & (CX)(CV) \\ CY & (CX)(CY) & CY^2 & (CY)(CZ) & (CY)(CV) \\ CZ & (CX)(CZ) & (CY)(CZ) & CZ^2 & (CZ)(CV) \\ CV & (CX)(CV) & (CY)(CV) & (CZ)(CV) & CV^2 \end{bmatrix} \times \begin{bmatrix} d[TE] \\ d[XE] \\ d[YE] \\ d[ZE] \\ d[VE] \end{bmatrix} = \begin{bmatrix} CR \\ (CR)(CX) \\ (CR)(CY) \\ (CR)(CZ) \\ (CR)(CV) \end{bmatrix} \tag{8}$$

where

$$N = 6 \qquad CZ = \sum_{i=1}^{6} \frac{(ZE-Z_i)}{VE \cdot D_i}$$

$$CX = \sum_{i=1}^{6} \frac{(XE-X_i)}{VE \cdot D_i} \qquad CV = \sum_{i=1}^{6} \frac{(-D_i)}{VE^2}$$

$$CY = \sum_{i=1}^{6} \frac{(YE-Y_i)}{VE \cdot D_i} \qquad CR = \sum_{i=1}^{6} (t_i - \hat{t}_i) \ .$$

We can obtain our first estimate of dS to be substituted into equation (5) by solving equation (8) using standard matrix inversion techniques. By repeating the process, using our improved estimates, we converge upon the solution.

A FORTRAN program performs the least-squares solution, giving as output for each event the space coordinates XE, YE, ZE of the hypocenter, the wave velocity VE, the event time TE, and the RMS time residual R. If the solution satisfies the criterion described below, the location, wave velocity, and event time as well as amplitude and first motion data are stored on digital tape for further computer analysis.

When a rock sample approaches failure, the acoustic emission rises dramatically and will often saturate the system. When this happens it is likely that the six channels will trigger on acoustic waves from two or more acoustic-emission events. The arrival times recorded for such bogus events will be meaningless. In general, the least-square solutions for such events will blow up and the computer program rejects the event.

Another type of error might occur when the p wave from a low-energy event triggers one or more of the nearest stations but is attenuated to such an extent that it does not trigger the farthest stations. These stations will often be triggered by the slower S-wave or by a wave reflected off the sample boundaries. These erroneous arrival times may cause the least-squares solution to blow up, in which case the event is rejected. Occasionally the program may converge to a solution. Such solutions will in general have large time residuals and are rejected on this basis. In addition, any event having a solution lying outside the sample or with unrealistically large or small velocities is rejected.

Because of these rejection criteria, only 10 to 20 percent of the events recorded in our experiments are accepted. With more careful analysis of raw data, we could improve this yield; however, it would dramatically increase computation costs. Furthermore, our present level of return provides ample data for numerical analysis. For example, in one eight-day experiment, 156,146 usable events were recorded.

Experimental Results and Discussion

In the experiment we report here, a sample of the Weber sandstone was subjected to a constant confining pressure of 1000 bars and a differential stress of 4000 bars. Water was injected at a constant pressure of 500 bars at one end of the sample.

The hypocenters of the acoustic-emission events that were recorded during the experiment were calculated by the method described above.

In order to obtain a visual representation of the event locations we project them onto a plane parallel to the long axis of the rock cylinder. In some of our experiments we have found that a well formed fault develops at failure. By projecting the event locations onto a plane normal to this fault plane, we can determine whether or not the events that were recorded during the experiment tended to cluster along the fault trace. Alternatively we can, by a least-square technique, calculate the plane that is a best fit to our data and then project our hypocenter locations onto a plane normal to this.

In the experiment that we report here, the least-square solution to our data gave a plane oriented at an angle of 130° to our coordinate system that is fixed by our piezoelectric transducer station locations. Our hypocenter locations were therefore plotted on the plane $\theta = 40°$.

We obtain a large amount of data and we have found that the most satisfactory way to represent it is to divide the projection plane into a grid, each cell of which has dimensions .255 x .42 cm. We then determine the number of events that occurred within each cell in the time interval of interest. The number of events occurring in each cell is expressed as a power of 2 in the computer printout.

Printout	Number of Acoustic Events
0	$N = 1$
1	$2 \leq N < 4$
2	$4 \leq N < 8$
3	$8 \leq N < 16$
.	.
.	.
.	.

Figure 2 shows a copy of the computer printout plot of the hypocenter locations of the events that occurred during the first 10,000 minutes plotted onto the plane $\theta = 40°$.

Representation of the data in this way is still not completely satisfactory because on reduction for publication purposes the numbers become too small to be legible. We have contoured the data shown in Figure 2 and presented this along with the contoured data collected during the rest of the experiment in Figure 3.

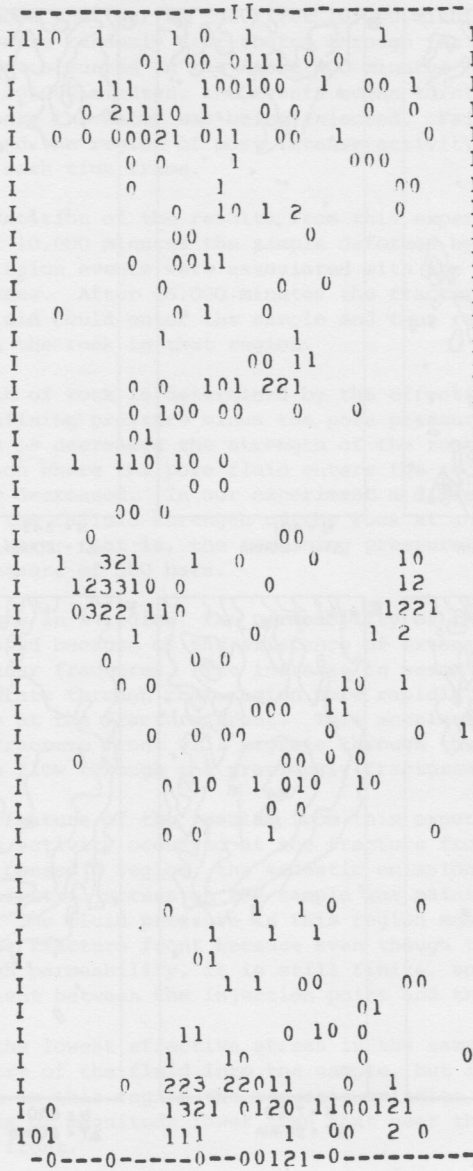

Fig. 2. Computer printout of the acoustic emission hypocenters projected onto a plane $\theta = 40°$. The numbers in the plot are the exponents to the base 2 of the number of events occurring within each grid cell. Each cell has dimensions 0.255 cm by 0.42 cm.

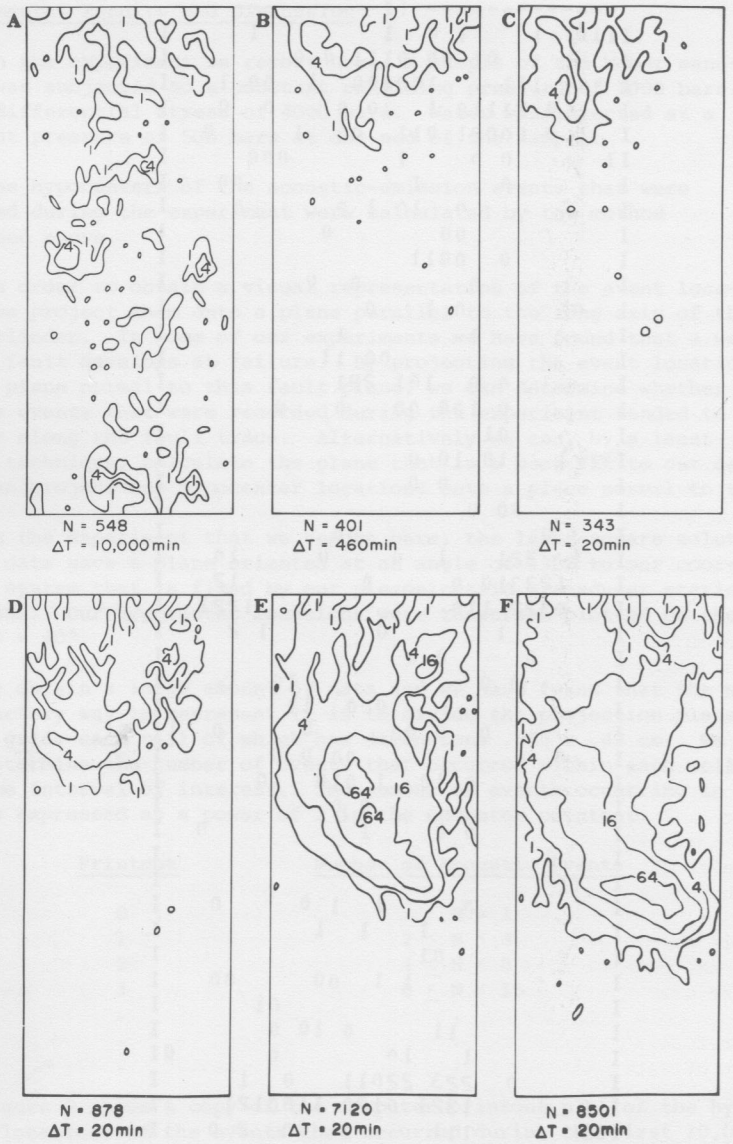

Fig. 3. Contours of hypocenter location density during the fluid injection experiment. The time interval and number of events are shown below each diagram. Differential stress throughout the experiment was 4 kb.

Figure 3 shows that during the first 10,000 minutes the acoustic-emission events were randomly distributed through the sample. Of these events, 75 percent occurred in the first 400 minutes of the experiment. After the first 10,000 minutes, the events began to cluster at the end of the sample where the water was being injected. Failure then proceeded rapidly and the region of most intense activity moved through the sample with each time frame.

Our interpretation of the results from this experiment is that during the first 10,000 minutes the sample deformed by creep and that the acoustic-emission events were associated with the formation of localized fractures. After 10,000 minutes the fracturing had reached a stage where fluid could enter the sample and thus reduce the effective pressure on the rock in that region.

The strength of rock is determined by the effective stress; that is, the confining pressure minus the pore pressure. As the effective stress is decreased the strength of the rock decreases. Thus in the region where the pore fluid enters the rock, the fracture strength will be decreased. In our experiment a differential stress of 4 kb exceeds the failure strength of the rock at an effective pressure of 500 bars; that is, the confining pressure of 1000 bars minus a pore pressure of 500 bars.

After failure in a region, the permeability of the rock in that region is increased because of the existence of extensive tension fractures and shear fractures. The increase in permeability allows the fluid to migrate through that region more rapidly, lowering the effective stress at the fracture front. This accelerates the fracturing and the fracture front will migrate through the sample as fast as the fluid can flow through the previously fractured material.

A striking feature of the results from this experiment is that the most intense activity occurred at the fracture front and that once this front passed a region, the acoustic emission decreased even though the differential stress on the sample was maintained at a constant value. The fluid pressure in this region must be higher than it is at the fracture front because even though the smashed-up material has high permeability, it is still finite, so there must be a pressure gradient between the injection point and the fracture front.

Therefore the lowest effective stress in the sample must be at the point of entry of the fluid into the sample, but in Figure 3F it can be seen that in this region the acoustic-emission activity is nearly two orders of magnitude lower than that near the leading edge of the fracture front.

A possible explanation for this phenomenon is that the acoustic emission associated with movement on the newly formed fault surfaces is much less than it is during the formation of the faults regardless of the level of effective stress.

Conclusions

In this paper we have restricted our attention to only one aspect of acoustic emission in rocks but with the system that we have described here it is possible to study other aspects besides the location of the acoustic-emission events.

For instance, with our system we can determine the seismic velocity, the source mechanism (whether tension fracture or shear fracture), the acoustic attenuation and the amplitude of the events at a fixed distance from the sources.

This paper is a progress report and we will publish the results of the other studies when they are completed. The work to date has shown that with the system we can study in fine detail the distribution of the hypocenters of the acoustic-emission events that occur during the injection of fluid into rock that is subjected to confining pressure and differential stress.

We hope that publication of this paper will help other workers in the field of rock mechanics who are in the process of developing a system to study acoustic emission in rocks.

REFERENCES

Liptai, R. B., D. O. Harris, and C. A. Tatro, An introduction to acoustic emission, in Acoustic Emission, American Society for Testing Materials, 1972, pp. 3-11.

Mogi, K., Source locations of elastic shocks in the fracturing process in rocks, Bulletin of the Earthquake Research Institute, 1968, v. 46, pp. 1103-1125.

Scholz, C. H., Experimental study of the fracturing process in brittle rocks, Journal of Geophysical Research, 1968, v. 73, pp. 1447-1454.